β-decay properties for neutron-rich Kr–Tc isotopes from deformed *pn*-quasiparticle random-phase approximation calculations with realistic forces

Dong-Liang Fang,[1,2] B. Alex Brown,[1,2,3] and Toshio Suzuki[4,5]

[1]*National Superconducting Cyclotron Laboratory, Michigan State University, East Lansing, Michigan 48824, USA*

[2]*Joint Institute for Nuclear and Astrophysics, Michigan State University, East Lansing, Michigan 48824, USA*

[3]*Department of Physics and Astronomy, Michigan State University, East Lansing, Michigan 48824, USA*

[4]*Department of Physics, College of Humanities and Sciences, Nihon University, Sakurajosui 3-25-40, Setagaya-ku, Tokyo 156-8550, Japan*

[5]*National Astronomical Observatory of Japan, Mitaka, Tokyo 181-8588, Japan*

(Received 26 November 2012; revised manuscript received 17 June 2013; published 16 August 2013)

In this work we studied β-decay properties for deformed neutron-rich nuclei in the region $Z = 36$–43. We use the deformed *pn*-QRPA (quasiparticle-random-phase approximation) methods with the realistic CD-Bonn forces, and include both the Gamow-Teller and first-forbidden types of decays in the calculation. The obtained β-decay half-lives and neutron-emission probabilities of deformed isotopes are compared with experiment as well as with previous calculations. The advantages and disadvantages of the method are discussed.

DOI: 10.1103/PhysRevC.88.024314 PACS number(s): 21.10.Tg, 21.30.Fe, 21.60.Ev, 23.40.Hc

I. INTRODUCTION

Decay properties such as the half-lives and β-delayed neutron emission probabilities are important inputs for the simulations of the *r*-process nucleosynthesis which is believed to be responsible for the production of heavy elements in our universe. In order to understand the observed elements abundance, one needs measurements together with models for making accurate predictions for these global properties of atomic nuclei out to the neutron driplines, especially those neutron-rich nuclei along *r*-process paths [1,2].

Recently, a group from RIKEN has performed a series of half-life measurements for the neutron-rich Kr-Tc isotopes [3]. For some of these nuclei, some differences from the previous measurement has been found, while for others, the half-lives are measured for the first time. These measurements give us more information for exotic neutron-rich nuclei and also offer us more information relevant for the *r*-process flow path around the $A = 130$ peak.

These new measurements serve as good tests or constraints for theories. The theory for such calculations from gross to microscopic have been developed for decades. There have been global estimations of half-lives from the gross theories such as those in Ref. [4] which treats the half-lives as functions of the Q values and proton (Z) and neutron (N) numbers. More microscopic methods have been developed in Ref. [1,5], with deformed *pn*-QRPA (quasi-particle-random-phase approximation) methods for Gamow-Teller (GT) type decays with the residual interaction from phenomenological *pn* forces in the $J^\pi = 1^+$ channel. Because of the phenomenological nature of the forces designed only for the GT channel, the first-forbidden (FF) part was estimated by gross theory instead of direct calculations [1]. Despite these approximations, Ref. [1] gives a reasonable average agreement with half-lives over the nuclear chart and for the new RIKEN data, but there are order-of-magnitude deviations between experiment and theory in many cases.

Reference [1] is the one that is widely accepted and used in astrophysical simulations. For this reason we will make comparisons to the results of [1]. There are other more recent calculations that we will comment on in comparison when appropriate. In a spherical basis with QRPA there have been improvements for the continuum effects [6], and the self-consistent density-functional theory (DFT) [7] has been used. In the deformed basis Ref. [8] made improvements with the introduction of particle-particle residual interactions and interactions in the negative parity channels, but the results are close to those of Ref. [1].

A new aspect of our method is that we use realistic forces for the residual interactions using the G-matrix formalism. This differs from the idea of using the same force everywhere in the calculation as in [7]; we will discuss why we think our approach is better. This method was first developed by the Tübingen group [9,10] for $\beta\beta$ decay to solve the problem of multi-spin-parity channels for neutrinoless $\beta\beta$-decay intermediate states. However, the idea of realistic forces to be used in the QRPA calculations can be traced back for decades. Previous publications for beta decay include the pioneer work of QRPA with realistic forces for β^+/EC calculation from Ref. [11], the ^{110}Cd β^--decay calculations in Ref. [12], and the comparison of low-lying spectra between shell model and QRPA calculations in Ref. [13]. Previous publications for double beta decay are more extended: they include [14,15] by the Tübingen group and [16] by the Jyvaskyla group. In all of these works, we see predictions which are comparable to the measurements and similar to the predictions from other methods. The advantage of this method is that we are not restricted to GT channels, and exact treatments of excitation energy are available. With just two parameters for the residual interactions, we can calculate all possible decay channels, such as the transitions from 0^+ ground states to $0^-, 1^-, 2^-$ final states. This gives explicit results from microscopic calculations for FF decays which in some nuclei may play an important role. On the other hand, inclusion of all spin-parities can give us better determinations of the spectra of odd-odd nuclei that make the decay energy required for phase-space factors much more accurate. Both are advantages which can lead to better predictions for β-decay properties.

This article is arranged as follows: in Sec. II we introduce the formulations of the calculations for β-decay properties and the many-body approach we adopt; in Sec. III the results and comparison to experiment and other models are discussed. The conclusions are given in Sec. IV.

II. FORMALISM

The half-lives of β-decaying isotopes can be expressed as

$$t_{1/2} = \ln 2/\Gamma, \tag{1}$$

where Γ is the decay width and has the form

$$\Gamma = \sum_j \Gamma_j = \sum_j \frac{1}{2\pi^3}\frac{m_e^5 c^4}{\hbar^7} \times \int_1^{\omega_j} \mathcal{C}(\omega) F(Z, R, \omega) p\omega(\omega_0 - \omega)^2 d\omega. \tag{2}$$

Here the sum runs over all the possible states j for the final nuclei, and $F(Z, R, \omega)$ is the phase-space factor for state j, which is a function of the nucleus radius R, nuclear charge Z, and the energies of the emitted electron $\omega_j = E_e/m_e = (Q - E_j)/m_e$ in units of the electron mass m_e. In this work, we consider two kinds of decays, the Gamow-Teller (GT) and first-forbidden (FF) decays. For GT decay, $\mathcal{C}(\omega) = B(\mathrm{GT}^-)$. It is the square of nuclear matrix elements describing the nuclear-structure part of the GT β decay, which can be expressed in the form

$$M_j = \langle j|\tau^+\sigma|i\rangle, \tag{3}$$

where $|i\rangle$ is the ground state for the parent nucleus and σ is the transition operator (Pauli matrices) for GT β decay. For the FF decay, the nuclear transition part $\mathcal{C}(\omega)$ has more complicated expressions as sums over products of different matrix elements, as presented in [17–20]:

$$\mathcal{C}(\omega) = K_0 + K_1\omega + K_{-1}/\omega + K_2\omega^2, \tag{4}$$

where K_0, K_1, K_{-1}, and K_2 are the nuclear matrix elements of various operators which depend on the multipoles, 0^-, 1^-, and 2^-. From the expression in (2) for the half-lives for decays to each final state, one needs the information for the excitation energies of the final states and the matrix element between the initial and final states. For different types of nuclei, we will use different many-body treatments as explained below.

Various methods have been applied to this calculation, each with some limitations. The large-basis shell model can account for many of the correlations, but the number of orbitals that can be considered is restricted by the computational limitations to dimensions of on the order of 10^{10}, and in practice is used only for the Gamow-Teller decay in light nuclei ($A \leqslant 60$). All of the nuclei considered here are outside of this range.

Thus one needs other methods that involve various approximations. In our case, we adopt the deformed version of pn-QRPA with realistic forces as first introduced in Ref. [9]. With the adiabatic Bohr-Mottelson approximation, one can prove the equivalence of the calculations performed in the laboratory systems and intrinsic systems [21] (in the intrinsic system, the z axis is attached to the symmetric axis of the nucleus). Thus we will perform our calculation in the intrinsic system without the consideration of rotations of the nucleus, and adopt the axially symmetric wave functions in the intrinsic frame. Details of the wave function calculation is described in Ref. [9] as well as the treatment of BCS pairing in the deformed nuclei. With the BCS pairing, one defines the Boglyubov quasiparticle creation and annihilation operators

$$\begin{pmatrix} \alpha_\tau^\dagger \\ \tilde{\alpha}_\tau \end{pmatrix} = \begin{pmatrix} u_\tau & v_\tau \\ -v_\tau & u_\tau \end{pmatrix} \begin{pmatrix} c_\tau^\dagger \\ \tilde{c}_\tau \end{pmatrix}, \tag{5}$$

where the annihilation operators annihilate the BCS vacuum, $\alpha_\tau|BCS\rangle = 0$. Here c and $c^\dagger$ are single-particle annihilation and creation operators, and u's and v's are BCS coefficients from the solutions of BCS equation.

The intrinsic excited states $|K^\pi, m\rangle$ are then generated by the QRPA creation operators acting on the ground states [10]:

$$|K^\pi, m\rangle = Q^\dagger_{K^\pi,m}|0^+_{g.s.}\rangle, \quad Q^\dagger_{K^\pi,m} = \sum_{p,n} X^m_{pn,K^\pi} A^\dagger_{pn,K^\pi} - Y^m_{pn,K^\pi}\tilde{A}_{pn,K^\pi}. \tag{6}$$

Here the two quasi particle creation and annihilation operators are defined as $A^\dagger_{pn,K^\pi} = \alpha^\dagger_p\alpha^\dagger_{\tilde{n}}$ and $\tilde{A}_{pn,K^\pi} = \alpha_{\tilde{p}}\alpha_n$, with the selection rule $K = \Omega_p - \Omega_n$. In order to obtain the forward and backward amplitudes X's and Y's, one needs to solve the QRPA equations

$$\begin{pmatrix} A(K^\pi) & B(K^\pi) \\ B(K^\pi) & A(K^\pi) \end{pmatrix} \begin{pmatrix} X^m_{K^\pi} \\ -Y^m_{K^\pi} \end{pmatrix} = \omega_{K^\pi,m} \begin{pmatrix} X^m_{K^\pi} \\ -Y^m_{K^\pi} \end{pmatrix}. \tag{7}$$

The expression of matrices A and B and the details of the interactions are discussed in Refs. [9,10]. The QRPA equations can be solved by diagonalizing following the method in Ref. [22]. The solutions contain the information of the energies from the eigenvalues and the structure information from the forward and backward amplitudes. With the states constructed from the solutions of QRPA equations, we can calculate the beta-decay half-lives. Here we briefly introduce the details of the calculations for different types of nuclei.

First, for the decays of even-even nuclei [the first even (odd) refers to the proton number Z and second even (odd) refers to the neutron number N], the parent nuclei have ground states with all the neutrons and protons paired. Thus it is the BCS vacuum with $J^\pi = 0^+$ (In intrinsic systems, the angular momentum is no longer conserved, but the projection on the z axis, K remains a good quantum number and the BCS vacuum is with $K^\pi = 0$). The excited states for daughter nuclei in the pn-QRPA formalism are just those we constructed above; we choose the states with the lowest eigenvalues to be the ground states of the corresponding odd-odd nuclei which are the decay products. (This requires a calculation over all the possible spin projections and parities K^π.) The excitation energies for each states are $E_{K^\pi,m} = \omega_{K^\pi,m} - \omega_{g.s.}$. The reason for such a choice instead of the direct use of QRPA energies is that with these excitation energies we can calculate the β-delayed neutron emission probability P_n. On the other side, due to the accuracy of QRPA solution, the obtained Q values from the parent side of excitations are less reliable than experimental measurements or some mass model

predictions. The matrix elements of the decay to the mth states with spin-parity K^π can then be derived as follows:

$$M^I_{K^\pi,m} = \langle K^\pi, m|O^I_M|0^+_{g.s.}\rangle = \sum_{pn} \delta_{KM}\langle p|O^I_M|n\rangle\left(X^m_{pn,K^\pi}u_p v_n + Y^m_{pn,K^\pi}v_p u_n\right). \tag{8}$$

Here $\langle p|O^I_M|n\rangle$ is the single-particle transition matrix element in the deformed basis, which can be written as a decomposition over the reduced matrix elements in spherical harmonic oscillator basis [9]: $\langle p|O^I_M|n\rangle = \sum_{\eta_p,\eta_n} F^{I'M}_{p\eta_p,n\eta_n}\langle\eta_p||O^I||\eta_n\rangle/\sqrt{2I+1}$. Here for GT decay the operator has the form $O^{GT}_K = \sigma_K\tau^+$ as we mentioned before, with the selection rules $\Delta K = 0, \pm1$ and $\Delta\pi = 1$, while the expressions for the first-forbidden beta decay are more complicated, with nine components with different spin-parities as introduced in Ref. [23]. We will not give the explicit expression for these components here, but mention that two have the selection rules $\Delta K = 0$, $\Delta\pi = -1$, three have the selection rules $\Delta K = 0, \pm1$, $\Delta\pi = -1$, and one has $\Delta K = 0, \pm1, \pm2$, $\Delta\pi = -1$.

For odd-mass nuclei, we follow the method in Ref. [1], except for the $\Delta v = 0$ case (defined in Ref. [21]), we consider only the single-particle transitions without the corrections from particle-vibration couplings for simplicity. The states of the odd-mass nuclei can be described as one corresponding quasiparticle (proton or neutron) excitation on the even-even ground states:

$$|Z \pm 1, N, i\rangle = \alpha^\dagger_{p,i}|Z, N, 0^+\rangle, \quad |Z, N \pm 1, i\rangle = \alpha^\dagger_{n,i}|Z, N, 0^+\rangle, \tag{9}$$

or a pn-QRPA excitation state with one spectator single particle (or hole):

$$|Z+1, N, I'm\rangle = \alpha^\dagger_{n,i}|K^\pi; m\rangle = \alpha^\dagger_{n,i}Q^\dagger_{K^\pi,m}|Z, N, 0^+\rangle, \quad |Z, N-1, I'm\rangle = \alpha^\dagger_{p,i}|K^\pi; m\rangle = \alpha^\dagger_{p,i}Q^\dagger_{K^\pi,m}|Z, N, 0^+\rangle. \tag{10}$$

Here the label i is the spectator nucleon which doesn't participate in the decay process. The ground states of these nuclei are the one-quasiparticle states with the lowest quasiparticle energies $E_{\tau,0}$; here τ can be a proton or neutron. Energies for the states in (9) are simply the differences between the quasiparticle energies $E = E_i - E_0$. For the states in (10), we use different treatments for the energies than that in Ref. [1]: $E = Q - Q_{EE} + E_m$; E_m is the actual pn-QRPA excitation energy in the even-even system and $Q - Q_{EE}$ accounts for the difference of the Q values between the odd-mass isotope and the corresponding even-even one. The matrix elements for the $\Delta v = 0$ single-particle transitions are then expressed as the leading order terms [21]

$$\langle Z+1, N, i|O^I_M|Z, N+1, 0\rangle = v_{p,i}v_{n,0}\langle p, i|O^I_M|n, 0\rangle, \quad \langle Z, N-1, i|O^I_M|Z-1, N, 0\rangle = u_{p,i}u_{n,0}\langle p, i|O^I_M|n, 0\rangle, \tag{11}$$

and for the $\Delta v = 1$ spectator case (also defined in Ref. [21]),

$$\langle Z+1, N, 0m|O^I_M|Z, N+1, 0\rangle = \sum_{p,n\neq n_0} \delta_{KM}\left(X^m_{pn,K^\pi}u_p v_n + Y^M_{pn,K^\pi}v_p u_n\right)\langle p|O^I_M|n\rangle,$$
$$\langle Z, N-1, 0m|O^I_M|Z-1, N, 0\rangle = \sum_{p\neq p_0,n} \delta_{KM}\left(X^m_{pn,K^\pi}u_p v_n + Y^M_{pn,K^\pi}TV_p u_n\right)\langle p|O^I_M|n\rangle. \tag{12}$$

Here contributions from the orbit occupied by the spectator particle (hole) are excluded.

Finally, we discuss the case of odd-odd nuclei following the treatment from Fig. 3 in Ref. [21]. In this scenario, the collective effect is excluded, and for the ground states of the odd-odd nuclei one has simply a one-neutron particle and a one-proton hole acting on the even-even ground states. For the daughter even-even nuclei, the ground states are obviously the BCS vacuum, while for the excited states, there exist two different types: the first case is the two-quasiparticle excitation neglecting the collectivity; the excitation energies are $E = E_{p,i} + E_{p,0}$ (lower left panel in Fig. 3 of Ref. [21]) or $E = E_{n,i} + E_{n,0}$ (upper right panel in Fig. 3 of Ref. [21]); the second case is the pn-QRPA excitation acting on the odd-odd ground; the energies are $E = Q - Q_{EE} + E_m$ (upper left panel in Fig. 3 of Ref. [21]), where Q_{EE} and E_m have the same meanings as in the odd-mass case. In the first case, the transition matrix elements are just those of (11) with one spectator proton hole or neutron particle. The special case is when the final states are the ground states with all neutrons and protons paired; in this case, the excitation energies are 0 instead of $2E_0$ (lower right panel in Fig. 3 of Ref. [21]).

The same matrix elements as in (12) are adopted with the exclusion of contributions from the orbits occupied by the unpaired neutron (particle) and proton (hole) of the odd-odd ground states. In this approximation, the result is independent of the odd-odd ground state spin, but the lack of collectivity will give an overestimation on the excitation energy of the two-quasiparticle final states. This makes the beta-decay Q values too low, and increases the beta lifetime. However, as discussed further below, the β-decay lifetimes for odd-odd nuclei are not so important for the r-process path.

The neutron emission probabilities are defined in Ref. [1] simply as

$$P_{\rm in} = \frac{\sum_{E_j > E_{\rm in}}\Gamma_j}{\Gamma}. \tag{13}$$

Here $P_{\rm in}$ is the i neutron emission probability, where i is the number of neutrons emitted and can be 1, 2, 3, or more, and $E_{\rm in}$ is the i neutron separation energy for i neutrons.

Following the definition in Ref. [1], the overall measure of error in the deviation of theory from experiment is defined by

$$r = \log_{10}\left(\frac{t_{1/2,\rm calc}}{t_{1/2,\rm exp}}\right), \quad \Sigma_r = \left[\frac{1}{n}\sum_{i=1}^{n}(r^i)^2\right]^{1/2}, \quad \Sigma^{10}_r = 10^{\Sigma_r}. \tag{14}$$

Here, Σ^{10}_r is defined to be the total "error." This will be used later for quantitative estimation of the quality of calculations.

III. RESULTS AND DISCUSSION

The single-particle wave functions and energy levels are obtained by solving the Schrödinger equation with the deformed Woods-Saxon potentials. The parameters of the Woods-Saxon potential are taken from Ref. [25]. For the choice of the model space, based on previous experience, we start from the $0\hbar\omega$ to one major shell above the Fermi surface of either proton or neutron, depending on which is close to zero energy, so for most isotopes here with $N \leqslant 70$, the model space is 0–5 $\hbar\omega$. For the deformation parameters, we choose either the experimental ones if available (using the treatment for deformation in Ref. [10]) or those predicted by Ref. [26]. The Q values and the neutron separation energies were taken from the experimental masses in Ref. [27], if available, and otherwise from the theoretical masses of Ref. [1]. For the pairing interaction, we adopt the Brückner G matrix with the charge-dependent Bonn force. The detailed calculation procedure and choice of parameters are described in Refs. [9,10,28]. The same interaction is used as the residual interaction for pn-QRPA phonons.

Ideally one would use the Skyrme or relativistic mean-field (RMF) method to generate both binding energies and single-particle energies self-consistently. In this paper we concentrate on the r-process beta-decay strengths which depend upon the use of reasonable single-particle energies and realistic residual interactions. For this purpose we use the same binding energies as used in previous finite-range droplet model (FRDM) calculations. We use single-particle energies obtained from a Woods-Saxon potential as stated above with parameters adjusted to observed single-particle energies in nuclei near stability (the present version of the deformed code is limited to a Woods-Saxon basis). For the future, all types of calculations for the single-particle energies in nuclei far from stability will need to include a consideration of the tensor component of the mean field that can modify the effective spin-orbit splittings [29].

As mentioned in the introduction, one of the new aspects of our work is the introduction of a microscopic calculation for the first-forbidden decays. Figure 1 shows the region of nuclei covered in this paper. For each nucleus we show the branching ratio for the forbidden decay. They vary from several percent to at most 30% in this region. Thus our discussions below apply mainly to the Gamow-Teller decay aspects of calculations. In other regions, the FF contributions are more important and an accurate determination of these decay widths can give a better accuracy; an example is given in [17] for $N = 126$ isotones where, for some isotones, the first-forbidden decays contribute more than 80% of the decay width. Overall, an explicit calculation of FF decay is required for a complete account of the beta-decay in the r-process path.

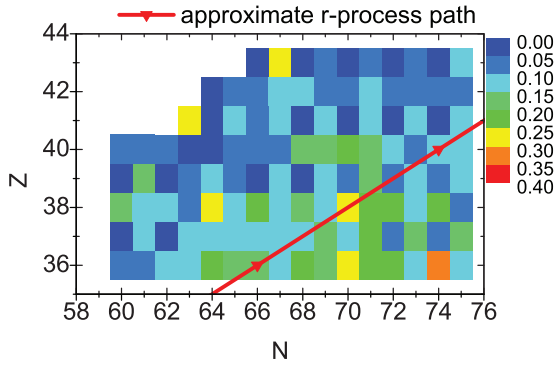

FIG. 1. (Color online) Illustrations of calculated branching ratios of the first-forbidden decay for different isotopes. The diagonal line indicates the approximate r-process path.

Two parameters are introduced as described in Refs. [9,10]: the renormalized particle-hole ($g_{\rm ph}$) and particle-particle ($g_{\rm pp}$) strengths. However, the fitting procedure of these parameters is a bit different from Refs. [9,10]. For the renormalized particle-hole strength $g_{\rm ph}$, the usual way is to fit the position of the Gamow-Teller resonance. Since we do not have enough data in the Kr-Tc region of interest, we adopt the same value as that derived in Ref. [9] for double-beta-decay emitter ^{76}Ge (In fact, the β decay depends on the low-lying strength distributions and the choice of $g_{\rm ph}$ does not affect the final results too much).

The calculated half-lives are sensitive to the renormalized particle-particle strength $g_{\rm pp}$. But we must also consider the possibility of quenching of the axial-vector coupling constant due to short-range correlations and to multiphonon effects which are excluded in QRPA calculations. Due to the lack of experimental data on $\log ft$ values of single-decay branches in our mass region of interest, we take the one used in Ref. [10] that was derived from experiment [30] for ^{150}Nd, $g_A = 0.75 g_{A0} = 0.95$, where $g_{A0} = 1.26$ is the bare value in the vacuum.

The relation between the calculated half-lives and values of $g_{\rm pp}$ is illustrated in Fig. 2. When $g_{\rm pp}$ is increased, we obtain an enhanced GT strength to low-lying states, and therefore smaller calculated half-lives. From Fig. 2 , we find that without quenching, the half-lives are underestimated, and the fitted $g_{\rm pp}$ values are around zero. If the quenching is included, realistic values from 0.6 to 0.9 which reproduce the half-lives of the

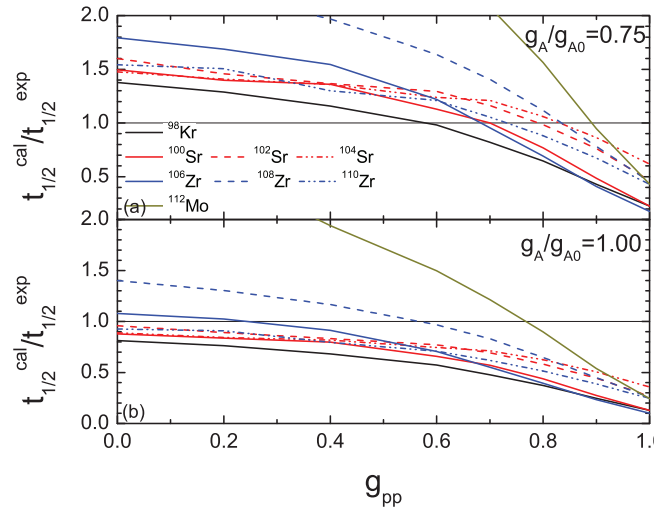

FIG. 2. (Color online) The half-life dependence on $g_{\rm pp}$ for different even-even isotopes. The upper panel shows results with quenched axial vector coupling constant $g_A = 0.75 g_{A0}$, while the lower panel shows the bare one $g_{A0} = 1.26$.

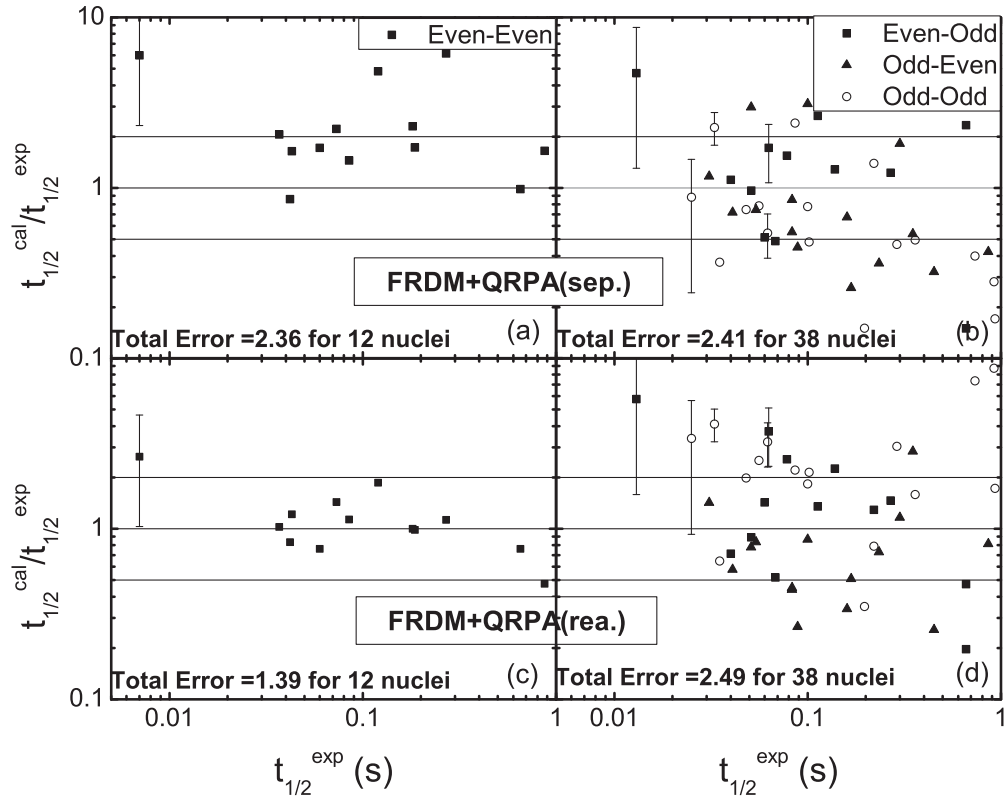

FIG. 3. A comparison of the calculated half-lives from Ref. [1] [(panels (a) and (b)] and this work [(panels (c) and (d)] with the experimental ones from RIKEN [3] and [24]. The experimental errors are taken into account for several isotopes with large error bars. The total errors are defined in (15). The left panels are comparison for even-even isotopes, and the right panels are for other types denoted by different symbols for the three cases of (Z, N). The three horizontal lines in each panel correspond to the ratios of 2, 1, and 0.5 respectively. Here, sep. is the abbreviation for separable force and rea. for realistic force.

isotopes are obtained; this agrees well with the fitted g_{pp} values of $\beta\beta$-decay half-lives in Ref. [10]. Due to the large uncertainty in half-life of ^{100}Kr we exclude this isotope from Fig. 1. Another isotope which is not included in the figure is ^{114}Mo, because it requires a larger model space due to its neutron number 72 (one more major shell should be added in the calculation compared with other isotopes), hence a much longer time is needed for calculation of the whole range of g_{pp}. However, as we shall see later, the results for ^{114}Mo agree well with those obtained with the $g_{pp} = 0.75$ value we choose from the fitting. For calculations in other deformed region, an A dependence of g_{pp} may be needed; however, in the current calculation in this region, a unified g_{pp} value seems to work well with our choice of model space.

With the uncertainties of the choice of g_{pp} from 0.6 to 0.9, the errors of the half-lives vary by a factor of 2 in general. The optimal choice is $g_{pp} = 0.75$ from the trends in the upper panel of Fig. 2. In Fig. 3, we show the ratio between calculated and measured half-lives with $g_{pp} = 0.75$. Following the definition from (15), we obtain a total error of 2.1 compared to 2.3 in Ref. [1] for all nuclei with lifetimes smaller than 1 s from Kr to Tc. If we compare our results with those obtained in Ref. [1] (upper panels in Fig. 3), we find that we have a better agreement for even-even nuclei (a total error of 1.39 compared to 2.36 for 12 nuclei with reasonably small error bars) not simply because we have adjusted the parameters for this region, but mainly due to the adaption of excitation energies relative to the ground states of the final odd-odd nuclei. This gives more accurate phase-space factors which effectively reduce the half-lives, and gives improved agreement with the experiment. For Ref. [1], even without the effect of quenching, there is an overestimation for almost all even-even nuclei due to the excitation energies they choose and the lack of particle-particle residue interaction in their calculation. For 38 odd-odd or odd-mass nuclei, a comparable total error is obtained between ours and that of Ref. [1].

A systematic analysis of the behavior for the GT distribution has been presented in Ref. [31] for the Zr and Mo even-even isotopes in this region. As an example, we show in Fig. 4 the low-lying GT and effective FF strength distributions for ^{110}Zr, in order to give a general idea of how the low-lying strength is distributed, and how they contribute to the decay width. General agreements have been achieved between our results in Fig. 4 and those of Fig. 5 for ^{110}Zr in Ref. [31] for GT strength distribution in units of g_{A0}^2, with differences coming from the different strength distributions which lead to different total GT strengths included in the decay window. We have a similar amount of total strength for both the spherical and deformed cases which is about 1.5 times of that for the spherical case and $\sim$2 times for the deformed case in Ref. [31]. If we compare the two scenarios, we have nearly the same amount of GT strength at the same position for the spherical

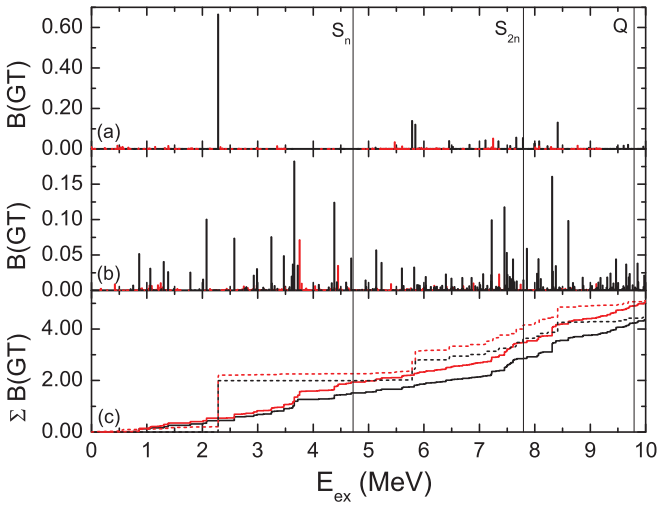

FIG. 4. (Color online) Low-lying GT (black) and effective FF (red) strength distributions (a), (b) and GT running sums (c) for ^{110}Zr are shown. The effective strength $\overline{C(w)}$ for first-forbidden decay is defined in Eq. (8) in Ref. [17]. In addition to the results in the deformed basis (b), we also show the results for a spherical basis (a) [dashed lines in (c)]. The three vertical lines correspond to $S_n = 4.72$ MeV, $S_{2n} = 7.79$ MeV, and $Q = 9.79$ MeV respectively, which are taken from Ref. [27]. Here, we use $g_{\rm pp} = 0.75$, which gives a half-life of $t_{1/2} = 21.6$ ms and β-delayed one-neutron emission probability $P_n = 1.9\%$ for the spherical case and $t_{1/2} = 37.9$ and $P_n = 10.5\%$ for the deformed case.

case, which leads to similar half-life and P_n for the spherical case, since only one transition dominates the decay width. The effect of deformation has also been explored by Ref. [31]. Here instead of a full analysis of the lifetime-deformation relation, we compared spherical case to the deformed case with only one deformation and obtained similar trends as that in Ref. [31]; that is, with deformation, the half-life gets longer. However, the change of half-life is less drastic than theirs, since our strength for the deformed case has been shifted down compared to theirs due to different excitation energy spectra. For the spherical case, we see the strength has been concentrated in several states because of the degeneracy between different projections of the angular momentum than that in Ref. [31]. Due to the deformations, the contributions are split into $K = 0$ and $K = \pm 1$ parts (under the intrinsic system, angular momentum is not a good quantum number); not only their energies but also the strengths. This makes the distribution spread out and the deformed nuclei decay slower than corresponding spherical ones. It also leads to a larger P_n value for the deformed case as some of the strength is shifted to the region above S_n. In Fig. 4, we show the position for Q value and the neutron separation energies. The strengths with the lowest excitation energies are most important to the decay width because of their larger phase spaces. Thus, although for the deformed case, nearly comparable amounts of GT strengths are located in the intervals of S_n–S_{2n} and S_{2n}–Q, the β-delayed two neutron emission probability P_{2n} is very small compared with P_n. In this sense, one needs both accurate predictions for the strengths and their positions. The advantage of realistic force is that it provides a better determination of the excitation energies. To see this, we presented some comparisons between our calculations and the limited experimental spectra in Table I for several states which are related to β decay. In the adiabatic approximation, the intrinsic excitations are decoupled from the rotations, and these exicitation energies are supposed to be the rotational band heads. The comparisons in Table I shows that with QRPA we could achieve errors of the excitation energies up to 1 MeV when compared with the measured spectra, which could give small deviations to the half-lives when the Q values are larger than several MeV.

In this work, we also added the FF parts in the graph to show how much the inclusion of first-forbidden decay will change the half-lives. We see that if the low-lying states turn out to be low-spin negative parity states, then the FF decays may become important as their relatively smaller effective strengths now are compensated by a large phase-space factor, which makes them comparable to the GT part. This can be seen in panel (c) of Fig. 4. For the spherical case (dashed lines), although the low-lying FF effective strength is very small, it still contributes about 20% to the total decay width just because it lies more than 1 MeV lower than the larger GT strength. The effect of increasing $g_{\rm pp}$ is that it enhances the low-lying strength and shifts down the excitation energies, hence reducing the half-lives. From the definition of P_n in Refs. [1,21], more low-lying strength below the neutron separation energies gives much smaller P_n values, and vice versa. Thus, a comparison with the experiments for both the half-lives and the P_n values is a good measure of how good the nuclear structure descriptions are. Comparison of our results to Ref. [31] and to experimental data in Fig. 3 show good agreements among different theories and experiments. In general, the errors for lifetimes in our calculations for even-even nuclei can be basically controlled within a factor of 2.

The agreement between experiment and theory for even-odd and odd-even isotopes is about a factor of 2 worse than that for even-even isotopes. The lack of particle-vibration coupling in calculations of matrix element in the odd-mass systems at this region does not seem to have too much effect on the final half-lives, however. This is consistent with the calculations in Ref. [1], where a weak-coupling approximation was assumed. But the particle-vibration coupling also affects the excitation energy by the mixing between the single-particle and collective states, which in turn changes the effective Q values, and finally the phase-space factors. As the phase-space factor has a Q value dependence of Q^5, this will leads to errors mentioned above.

The agreement between experiment and theory is worse for the odd-odd isotopes, and there exists a systematic overestimation for the half-lives. This is due to a shortcoming of the method we use: the lack of consideration of the collectivity for even-even daughter nuclei. This overpredicts the energies of the final states, and hence the calculated phase factors are smaller than expected. However, in spite of the shortcoming of the methods, we can still keep the error within an order of magnitude, and for most isotopes approximately a factor of 5. We note from [32] that the r-process path does not depend strongly on the beta-decay properties of the odd-odd nuclei due to their larger S_n values. Thus, instead of improving the models for odd-odd nuclei, one alternative way

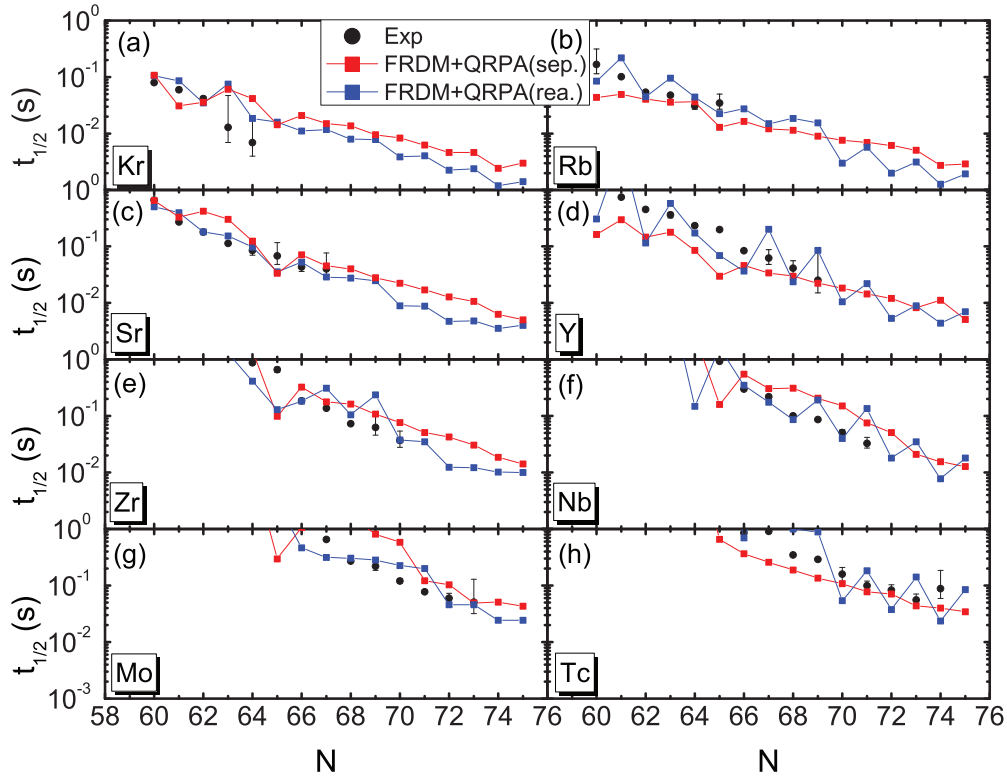

FIG. 5. (Color online) A comparison among the calculated half-lives from Ref. [1] (red), this work (blue), and measured ones (if available) with error bars from RIKEN [3] for Kr to Tc isotopes. The total errors are defined in Ref. [1]. Here, as before, sep. is the abbreviation for separable force and rea. for realistic forces.

is to simply use the average of the results for the neighboring odd-even and even-odd nuclei for their values in an *r*-process database.

With the above comparisons and discussions, we extend our calculations to all of the deformed Kr-Tc isotopes in the region $N = 50$–82. We make comparisons with experimental measurement (if available) and previous theoretical predictions from Ref. [1]. The results are shown in Fig. 5. The same set of Q values taken from FRDM model as used in Ref. [1] is adopted for the sake of comparison. One of the differences between our results and that of Ref. [1] is that the latter have added an extra strength spreading for each of the final states. In our calculations of even-even nuclei the strength is already spread by the deformation effects as seen above, and there is not as much motivation for adding more by hand. But for our calculations of odd-mass and odd-odd nuclei where the collective behavior has been excluded, the transitions are just between the single-particle states with little spreading compared to that in Fig. 4 for even-even nuclei.

TABLE I. The excitation enegies of the first 1^+, 0^-, 1^-, 2^- states in units of MeV from our calculations and from the experimental measurements of nuclei which are supposed to be deformed. The calculated ground state spin-parities are also shown.

		$J^\pi_{g.s.}$	$E_{1^+_1}$	$E_{0^-_1}$	$E_{1^-_1}$	$E_{2^-_1}$
^{98}Y	Expt.	0^-	0.548	0	0.119	0.171
	Theor.	4^+	0.108	0.014	0.194	0.395
^{100}Y	Expt.	$1^-, 2^-$	0.011		0	0
	Theor.	5^-	0.343	0.130	0.450	0.991
^{100}Nb	Expt.	1^+	0			
	Theor.	4^-	0.234	0.461	0.114	0.267
^{108}Tc	Expt.	2^+	0.086			
	Theor.	0^+	0.027	0.404	0.300	0.269

For most even-even isotope chains, shorter half-lives by up to a factor of 2 are predicted in our calculation compared to Ref. [1] due to the lower excitation energies for the final states from realistic calculations. This behavior applies also to some odd-mass nuclei. For even Z isotopes, the half-lives decrease with the increase of neutrons with some small staggering behavior, but overall agreement with experiment is obtained. For odd Z, there are systematic overestimations of the half-lives for the odd-odd isotopes with the reasons stated in Sec. II. For the odd-even nuclei, the agreement once again seems satisfying, however, we do find worse agreement for Tc isotopes, this may imply that these nuclei lies in the transitional region and a deformed QRPA description may not be proper for these isotopes. In Ref. [1], due to the additional strength spreading put in by hand, they obtained better agreements for these isotopes. However, if we observe carefully, we will see that although this artificial spreading of strength does smooth the behavior of the isotope chains, it may introduce further errors as in Fig. 5. With a unified value of spreading strength width, some results for isotope chains are overestimated while others are underestimated, and the rest curves have different

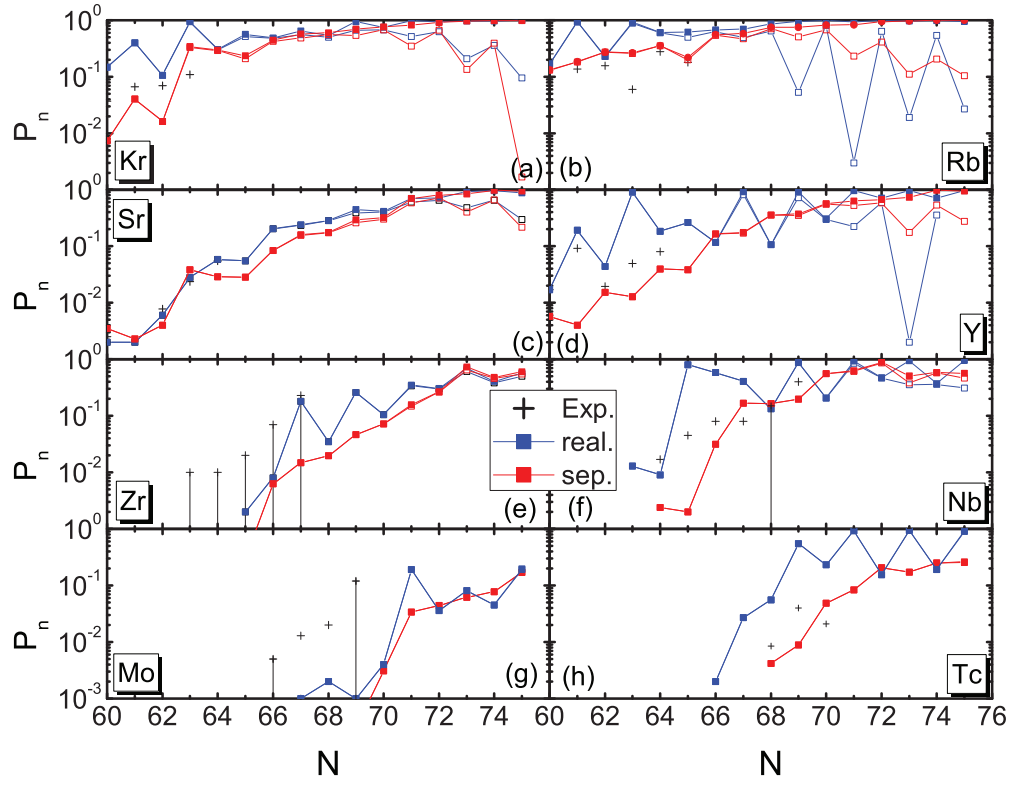

FIG. 6. (Color online) A comparison among the calculated β-delayed neutron emission probability P_n values from Ref. [1] (red), this work (blue), and measured ones (if available) with error bars from RIKEN [3] for Kr to Tc isotopes. Here sep. is the abbreviation for separable force and rea. for realistic forces. The empty squares are the β-delayed one-neutron emission probabilities P_n, while the solid ones are the total probabilities up to three-neutron emission.

slopes compared to the experimental results. It seems that one needs to adjust this value for each isotope chains to obtain a better agreement, hence it is not practical for global calculation if one would like to control the systematic errors of the calculations. This is why we have not added this spreading effect in our calculations. As discussed in Sec. II, the r-process results are not sensitive to the half-lives of the odd-odd nuclei, and from a practical point of view it would be adequate to simply use the average of the calculated half-lives of the neighboring even nuclei for these odd-odd nuclei, since we have generally good agreement with experiment for nuclei with even N or Z.

Another observable from the experiments for some isotopes is the P_n value, which with accurate neutron separation energies gives a measure of the Gamow-Teller strength distribution as we have shown in Fig. 4. From Fig. 6, we find a good agreement again for even-even isotopes from limited data, proving the reliability of our descriptions for deformed even-even isotopes in this region. In Fig. 6, one finds a staggering behavior in the realistic results for the even and odd N number neutrons, especially for the odd Z isotopes. The reason can be traced back to the treatment of the odd nuclei with the lack of collectivity. This shifts the excitation energies up and the strength distributions are shifted systematically to higher energies. This behavior is more obvious for odd-odd nuclei where nearly all the strengths are shifted up. In applications of our calculations to the r process, it is preferable to replace the calculated P_n results for odd N values with the average of the neighboring even N values.

IV. IMPLICATIONS FOR THE r PROCESS

We have investigated how the r-process element abundances are affected by the β-decay half-lives of various nuclei by changing the half-lives of Moeller's predictions [1] for all even-even or odd-odd nuclei by one order of magnitude. These preliminary results agrees with recent r-process simulations [32]: for even-even nuclei, such changes of lifetimes have a tremendous effect on the peak formations, totally changing the patterns of the abundance distributions. In the case of odd-odd nuclei, a one-order-of-magnitude change in all of the half-life results essentially keeps the same r-process abundance pattern, except for the $A = 150$–200 mass region where the odd-even oscillation for elemental abundances are relatively changed by about a factor of 2.

We can conclude from this simple simulation that the current accuracy of the deformed QRPA method can meet the needs of nuclear inputs for the r-process simulation. Our next step is to extend the present calculations to other deformed regions; for example, the heavily deformed rare-earth elements region, where the beta-decay data is limited, and where it is still not understood how the peak of rare-earth elements is formed. The final goal is to calculate the β-decay properties

over the whole nuclear chart. It is also important to have reliable calculations for spherical nuclei, especially those around $N = 82$ that are important for the abundance peak around $A = 130$.

V. CONCLUSION

In this work, we investigated the β-decay properties of the Kr-Tc isotopes recently measured at RIKEN. With the *pn*-QRPA taking into account realistic forces, a good agreement has been obtained between the theory and the experiments, especially for even-even nuclei, with an accuracy within a factor of 2 for most of them. The current calculations provide improved results for the beta-decay half-lives of even-even nuclei. We plan to apply the present method to the rare-earth region of deformed nuclei. We also plan to use the realistic interactions for QRPA calculations of spherical nuclei. This will eventually provide an improved set of predictions for the half-lives and P_n values that can be used in r-process network calculations for the element abundances.

ACKNOWLEDGMENT

This work was supported by the US NSF (PHY-0822648 and PHY-1068217).

[1] P. Moller, B. Pfeiffer, and K.-L. Kratz, Phys. Rev. C **67**, 055802 (2003).
[2] S. Wanajo, S. Goriely, M. Samyn, and N. Itoh, Astrophys. J. **606**, 1057 (2004).
[3] S. Nishimura, Z. Li, H. Watanabe, K. Yoshinaga, T. Sumikama, T. Tachibana, K. Yamaguchi, M. Kurata-Nishimura *et al.*, Phys. Rev. Lett. **106**, 052502 (2011).
[4] K. Takahashi and M. Yamada, Prog. Theor. Phys. **41**, 1470 (1969).
[5] J. Krumlinde and P. Moller, Nucl. Phys. A **417**, 419 (1984).
[6] I. N. Borzov, Phys. Rev. C **67**, 025802 (2003); J. J. Cuenca-Garcia, G. Martinez-Pinedo, K. Langanke, F. Nowacki, and I. N. Borzov, Eur. Phys. J. A **34**, 99 (2007).
[7] J. Engel, M. Bender, J. Dobaczewski, W. Nazarewicz, and R. Surman, Phys. Rev. C **60**, 014302 (1999).
[8] H. Homma, E. Bender, M. Hirsch, K. Muto, H. V. Klapdor-Kleingrothaus, and T. Oda, Phys. Rev. C **54**, 2972 (1996).
[9] M. S. Yousef, V. Rodin, A. Faessler, and F. Simkovic, Phys. Rev. C **79**, 014314 (2009).
[10] D.-L. Fang, A. Faessler, V. Rodin, and F. Simkovic, Phys. Rev. C **83**, 034320 (2011).
[11] J. Suhonen, T. Taigel, and A. Faessler, Nucl. Phys. A **486**, 91 (1988).
[12] M. Bertschy, S. Drissi, P. E. Garrett, J. Jolie, J. Kern, S. J. Mannanal, J. P. Vorlet, N. Warr *et al.*, Phys. Rev. C **51**, 103 (1995); **52**, 1148(E) (1995).
[13] A. Holt, T. Engeland, E. Osnes, M. Hjorth-Jensen, and J. Suhonen, Nucl. Phys. A **618**, 107 (1997).
[14] O. Civitarese, A. Faessler, and T. Tomoda, Phys. Lett. B **194**, 11 (1987).
[15] G. Pantis, F. Simkovic, J. D. Vergados, and A. Faessler, Phys. Rev. C **53**, 695 (1996).
[16] J. Toivanen and J. Suhonen, Phys. Rev. Lett. **75**, 410 (1995).
[17] T. Suzuki, T. Yoshida, T. Kajino, and T. Otsuka, Phys. Rev. C **85**, 015802 (2012).
[18] E. K. Warburton, J. A. Becker, B. A. Brown, and D. J. Millener, Ann. Phys. (NY) **187**, 471 (1988); H. Behrens and W. Bühring, Nucl. Phys. A **162**, 111 (1971).
[19] H. Schopper, *Weak Interactions and Nuclear Beta Decays* (North-Holland, Amsterdam, 1966).
[20] I. S. Towner and J. C. Hardy, Nucl. Phys. A **179**, 489 (1972).
[21] P. Moller and J. Randrup, Nucl. Phys. A **514**, 1 (1990).
[22] P. Ring and P. Schuck, *The Nuclear Many Body Problem* (Springer-Verlag, Berlin, 1980).
[23] H. A. Weidenmuller, Rev. Mod. Phys. **33**, 574 (1961).
[24] http://www.nndc.bnl.gov/chart/
[25] R. Nojarov, Z. Bochnacki, and A. Faessler, Z. Phys. A **324**, 289 (1986).
[26] S. Goriely, N. Chamel, and J. M. Pearson, Phys. Rev. Lett. **102**, 152503 (2009).
[27] G. Audi, A. H. Wapstra, and C. Thibault, Nucl. Phys. A **729**, 337 (2002).
[28] V. A. Rodin, A. Faessler, F. Simkovic, and P. Vogel, Nucl. Phys. A **766**, 107 (2006); **793**, 213(E) (2007).
[29] B. A. Brown, T. Duguet, T. Otsuka, D. Abe, and T. Suzuki, Phys. Rev. C **74**, 061303 (2006).
[30] C. J. Guess, T. Adachi, H. Akimune, A. Algora, S. M. Austin, D. Bazin, B. A. Brown, C. Caesar *et al.*, Phys. Rev. C **83**, 064318 (2011).
[31] P. Sarriguren and J. Pereira, Phys. Rev. C **81**, 064314 (2010).
[32] R. Surman (private communication).